Journal of Materials Chemistry A

Polypyrrole-Encapsulated Amorphous Bi2S3 Hollow Sphere for Long Life Sodium Ion Battery and Lithium-Sulfur Battery

Journal:	*Journal of Materials Chemistry A*
Manuscript ID	TA-ART-02-2019-001358.R1
Article Type:	Paper
Date Submitted by the Author:	08-Mar-2019
Complete List of Authors:	Long, Bei; Sun Yat-Sen University Qiao, Zhengping; Sun Yat-sen University, Chemistry and Chemical Engineering Zhang, Jingnan; Sun Yat-sen University, School of Material Science and Engineering Zhang, Shanqing; GRIFFITH UNIVERISTY, Griffith School of Environment Balogun, M.-Sadeeq (Jie Tang); Hunan University, College of Materials Science and Engineering Lu, Jun; Argonne National Laboratory, Chemical Science and Engineering Division Song, Shuqin; Sun Yat-sen University, School of Physics and Engineering Tong, Yexiang; Sun Yat-Sen University, School of Chemistry and Chemical Engineering

Journal Name

ARTICLE

Polypyrrole-Encapsulated Amorphous Bi_2S_3 Hollow Sphere for Long Life Sodium Ion Battery and Lithium-Sulfur Battery

Received 00th January 20xx,
Accepted 00th January 20xx

DOI: 10.1039/x0xx00000x

www.rsc.org/

Bei Long,[a] Zhengping Qiao,[a] Jingnan Zhang,[a] Shanqing Zhang,[c] Muhammad-Sadeeq Balogun,[d] Jun Lu,*[b] Shuqin Song*[a] and Yexiang Tong*[a]

Abstract: Sodium ion battery (SIB) and lithium-sulfur (Li-S) battery are considered as the most promising next-generation energy storage devices to displace the widely used lithium ion battery due to their inherent advantages. Here, the polypyrrole-encapsulated amorphous Bi_2S_3 hollow sphere is prepared by the sulfuration of Bi-glycol sphere with polypyrrole (PPy) coating. Benefiting from the unique hollow structure (Kirkendall Effect) and the excellent conductivity and flexibility of PPy coating, this material can be applied in both SIB and Li-S battery. For SIB, the unconductive amorphous Bi_2S_3 is electrochemically reduced to conductive metallic Bi, leading to a Bi-PPy core-shell structure. The resulting Bi acts as main active material while the PPy coating accommodates the volume variation of Bi during sodiation/desodiation. For Li-S battery, the outer double layer structure effectively prevents the dissolution and "shuttle effect" of polysulfides by physically containing and chemically adsorbing polysulfides and tolerates the volume expansion of sulfur. Meanwhile, the residual polyvinyl pyrrolidone in preparation process chemically bonding with sulfur exhibits the electrochemical properties and results in an additional discharging/charging capacity. Thus, this multifunctional electrode shows excellent rate capability and cycling life in SIB and Li-S battery. This work provides a new insight into the design of multifunctional electrode.

Introduction

The rapid consumption of lithium source and the demand of advanced energy storage devices with higher energy density prompt the search of a promising candidate of lithium ion battery.[1-9] Owing to the low cost and rich reserve of sodium and sulfur, sodium ion battery (SIB), which has similar intercalation chemistry to lithium, and lithium-sulfur (Li-S) battery with high theoretical energy density of 2600 Wh kg^{-1}, 5-fold higher than the commercialized lithium ion battery, show great prospect for next-generation energy storage devices.[10-15] However, the development of SIB is hindered because the larger size of Na^+ than Li^+ results in the depressed reaction dynamics and the severe volume variation of electrode during sodium intercalation/deintercalation.[16-18] Also, the poor conductivity of sulfur, the generation of dissoluble intermediate lithium polysulfides (LiPSs) and the "shuttle effect" of LiPSs as well as the ≈80% volume variation of sulfur cathode during lithiation/delithiation hamper the commercial application of Li-S battery.[19-21]

The ingenious structure design of electrode material is an effective method to solve these problems.[22-27] Porous and hollow structures often are used to accommodate the volume change of electrode and achieve a rapid charge transfer.[28-30] For example, Lou's group reported that $Cu_{1.8}S$ hollow octahedron could provide enough space for sodium intercalation, accelerate charge transfer rate and show a long-term cycling stability.[28] Zhong *et al.* used porous macrocellular carbon to prevent the dissolution and the "shuttle effect" of LiPSs and confine the volume variation of S during charging/discharging process.[29] On the other hand, the electrode pulverization and the poor electronic conductivity of semiconductor and S can be significantly addressed by the modification of various carbon and conductive polymer.[31-33] Chen and his colleagues prepared carbon-coated bimetallic sulfide hollow nanocubes as anode of SIB and its electrochemical performances outperformed the sulfide without protective carbon layer.[31] Mei *et al.* designed the porous carbon-coated Ti_4O_7 particles to confine the volume expansion of S and accelerate the Li^+ and the electrons transfer, and thus porous carbon-coated Ti_4O_7-S cathode exhibited the better cyclic stability than that of non-carbon coated Ti_4O_7-S.[32] It is noteworthy that these modification methods in SIB and Li-S battery are extremely similar. This is, these well-designed materials for SIB may be applied in Li-S battery and vice versa. Nevertheless, there rarely are the reported electrode material

[a.] The The Key Lab of Low-Carbon Chemistry & Energy Conservation of Guangdong Province, MOE of the Key Laboratory of Bioinorganic and Synthetic Chemistry, KLGHEI of Environment and Energy Chemistry, School of Materials Science and Engineering, School of Chemistry, Sun Yat-sen University, Guangzhou 510275 P. R. China. E-mail: S.Q. Song: stsssq@mail.sysu.edu.cn; Y.X. Tong: chedhx@mail.sysu.edu.cn
[b.] Chemical Sciences and Engineering Division, Argonne National Laboratory, Argonne, Illinois 60439, USA. E-mail: junlu@anl.gov
[c.] Centre for Clean Environmental and Energy and School of Environment and Science, Griffith University, Gold Coast, Queensland, 4222, Australia
[d.] College of Materials Science and Engineering, Hunan University, Changsha 410012 P. R. China

Electronic Supplementary Information (ESI) available: [details of any supplementary information available should be included here]. See DOI: 10.1039/x0xx00000x

which can be applied in both SIB and Li-S battery and show excellent electrochemical performances.

As a typical alloying reaction material, the metal Bi can react with multiple Na^+ and has a relatively high theoretical capacity (385 mAh g^{-1} and 1075 mAh cm^{-3}) compared to carbon-based anode and a suitable working voltage (below 1.0 V) in SIB.[34, 35] Meanwhile, compared to Sn (423%), P (440%) and Sb (390%), its small volume expansion (250%) makes the metal Bi exhibit a long cycling stability.[34, 35] Thus, metal Bi-based materials have been widely studied recently.[34-37] In previous reports, Bi@graphite composite exhibited an ultralong cyclic life with 90% capacity retention at 3200 mA g^{-1} after 10000 cycles but a low discharge capacity with 160 mAh g^{-1} at 160 mA g^{-1}.[36] By contrast, bulk Bi coupling with glyme-based electrolytes delivered an excellent rate capability (356.0 mAh g^{-1} at 2000 mA g^{-1}) but a relatively short cycling life (2000 cycles).[37] Therefore, it is very important to find an advanced Bi-based material with a long-term stability and a high rate capability. On the other hand, many metal sulfides have been considered as an outstanding adsorbent which can prevent the dissolution and the "shuttle effect" of polysulfides such as WS_2 and Co_9S_8 so far.[38, 39] So, bismuth sulfide with polar bonds may also act as S host in Li-S battery.

In view of this, we fabricate an amorphous Bi_2S_3 hollow sphere coated with polypyrrole (denoted Bi_2S_3-PPy HS) as an anode materials of SIB and sulfur host of Li-S battery by the sulfuration of PPy-coated Bi-glycol sphere for the first time. The Kirkendall Effect leads to the generation of hollow structure which is beneficial for the large contact surface area between active materials and electrolyte as well as the accommodation of volume change in the charging/discharging processes. The conductive PPy coating not only accelerates the electrons conduction but also physically bind the Bi_2S_3 nanoparticles together, maintain electrode integrity, contain electroactive materials and prevent electrode pulverization. The polyvinyl pyrrolidone (PVP) is combined with S by chemical bond and displays the electrochemical activity. It can be envisaged that the as-designed Bi_2S_3-PPy HS exhibits excellent rate capability and cycling stability in both SIB and Li-S battery.

Result and discussion

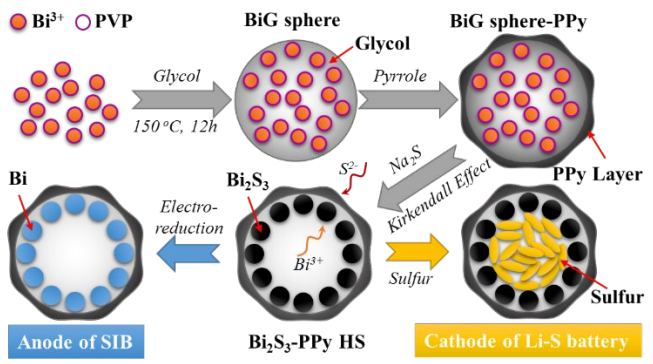

Fig. 1 Schematic illustration of the preparation of the amorphous Bi2S3-polypyrrole hollow sphere (Bi_2S_3-PPy HS) electrode.

Schematic illustration for the synthesis and application of multifunctional electrode is depicted in Fig. 1. In brief, the BiG sphere is prepared by one-pot hydrothermal method. The formation mechanism of BiG sphere is discussed in Supporting Information (Fig. S1). After BiG sphere is coated with a thin layer of PPy followed by sulfuration, the well-designed Bi_2S_3-PPy HS is obtained. During sulfuration process, S^{2-} ions in aqueous solution react with the superficial Bi^{3+} of BiG sphere firstly. And then the reaction of the inward diffusing S^{2-} and outward faster Bi^{3+} of BiG sphere occurs and glycol is dissolved in water, resulting in the generation of amorphous Bi_2S_3 hollow sphere (Kirkendall Effect). Such a nanomaterial is reported firstly. When it is electroreduced to metallic Bi-PPy composite, it becomes an excellent anode in SIB. While it is mixed with moderate amounts of sulfur, it can act as superior cathode in Li-S battery. The specific preparation process can be seen in experimental section. Fig. 2a shows the X-ray diffraction (XRD) patterns of Bi_2S_3 HS and Bi_2S_3-PPy HS. Two weak characteristic peaks at 25.9° and 30.1° are ascribed to amorphous Bi_2S_3.[40, 41] In Raman spectra (Fig. 2b), the characteristic peaks at 71.5, 100.3 and 237.8 cm^{-1} are attributed to the A_g mode of Bi_2S_3 and the peak at 262.2 cm^{-1} corresponds to B_{1g} mode of Bi_2S_3.[42, 43] These reflect the generation of amorphous Bi_2S_3. The successful coating of PPy can be proved by Raman and X-ray photoelectron spectroscopy (XPS) spectra. Two obvious peaks at 1367.7 and 1576.9 cm^{-1} are ascribed to pyrrole ring and C=C bonds, respectively (Fig. 2c).[44] Compared to the ignorable signal of Bi_2S_3 HS, the strong N 1s XPS peak of Bi_2S_3-PPy HS is derived from PPy coating (Fig. 2d). Surprisingly, a weak peak at 1441.7 cm^{-1} can be observed in Raman spectrum of Bi_2S_3 HS (Fig. 2c). Meanwhile, the elemental mappings show the even distribution of element C on Bi_2S_3 HS (Fig. S2). These reveal the remaining PVP in Bi_2S_3 HS.

Scanning electron microscope (SEM) and transmission electron microscope (TEM) reveal the morphology evolution of Bi-based materials. BiG sphere is a smooth and not hollow sphere, as shown in Fig. 3a,b and S3a,b. After sulfuration, the

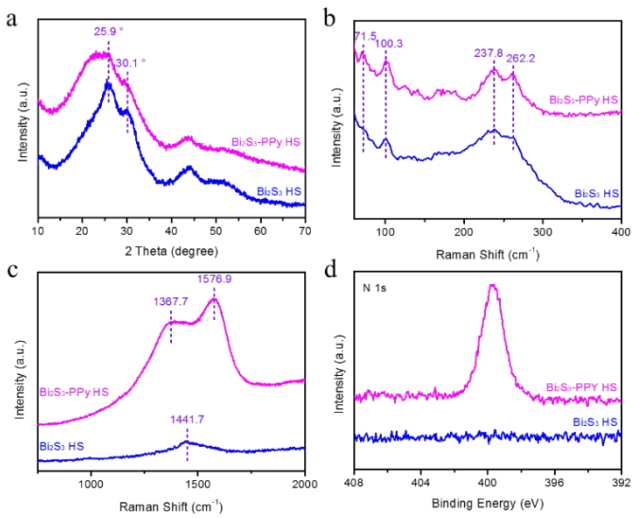

Fig. 2 (a) The XRD patterns, (b,c) Raman spectra and (d) N 1s XPS spectra of Bi_2S_3 HS and Bi_2S_3-PPy HS.

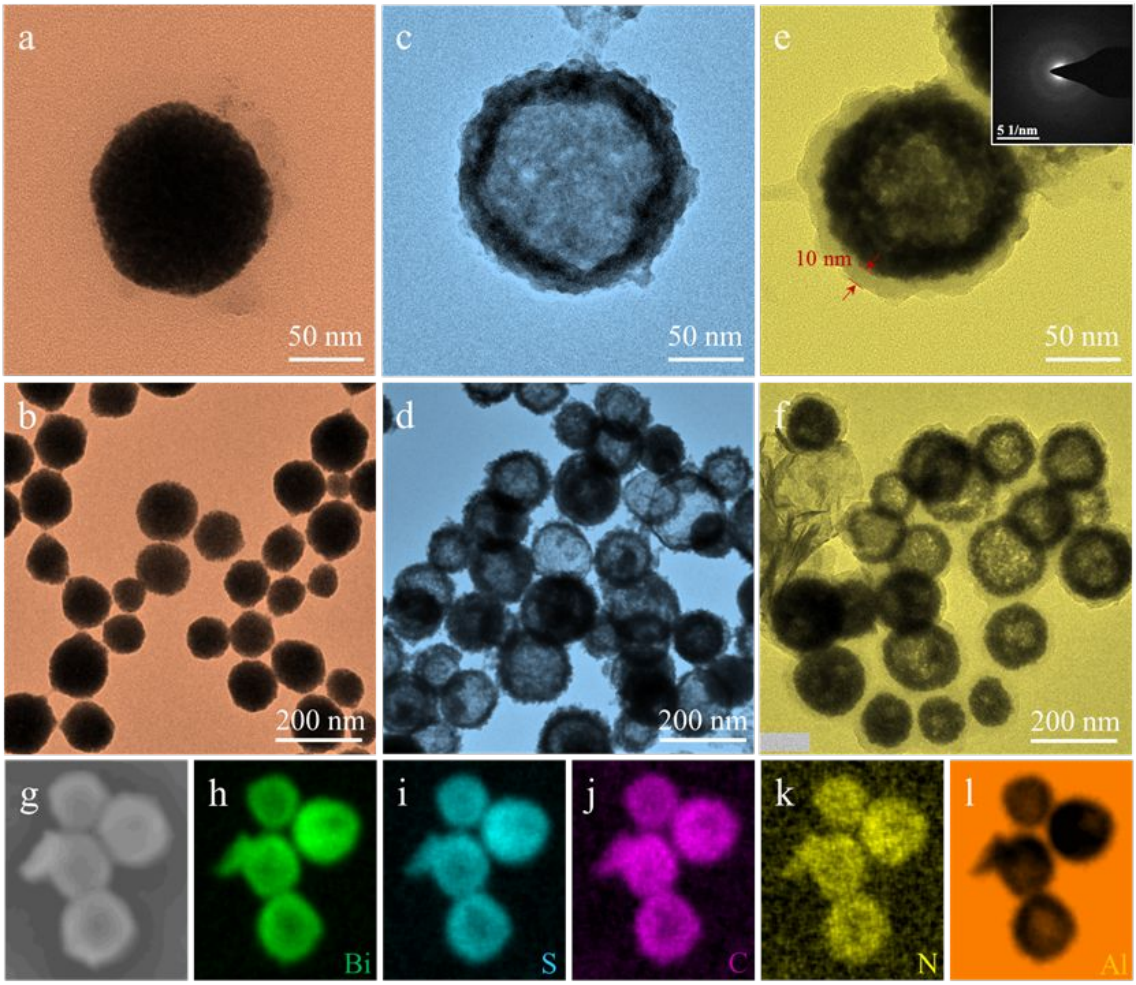

Fig. 3 TEM images of (a,b) BiG sphere, (c,d) Bi_2S_3 HS and (e,f) Bi_2S_3-PPy HS. (g-l) Elemental mappings of Bi_2S_3-PPy HS (Al came from substrate).

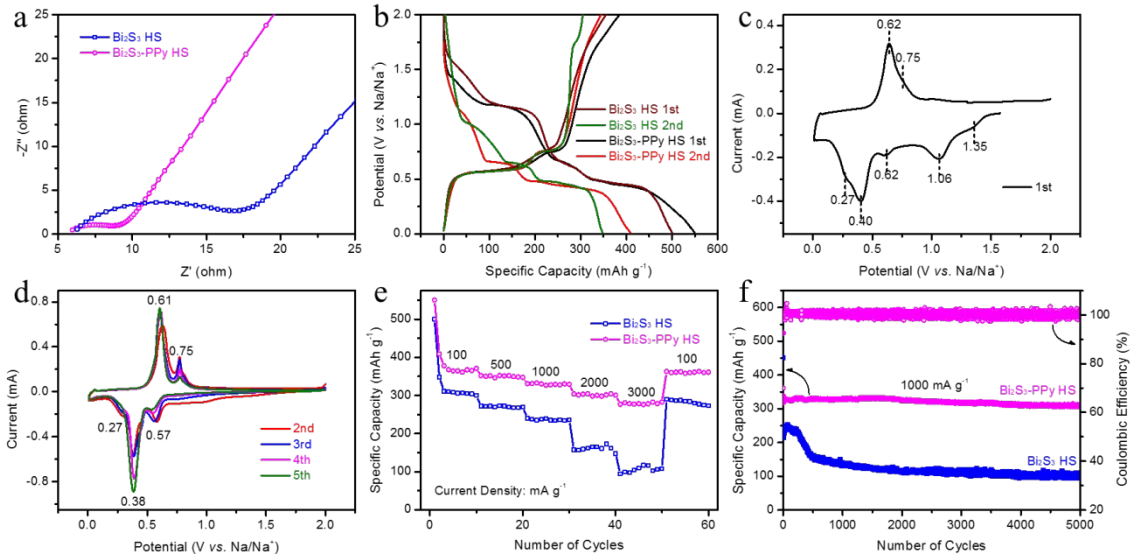

Fig. 4 (a) EIS spectra of Bi_2S_3 HS and Bi_2S_3-PPy HS. (b) The first and second charging-discharging curves of Bi_2S_3 HS and Bi_2S_3-PPy HS. CV curves of (c) first cycle and (d) 2nd-5th cycles for Bi_2S_3-PPy HS at scan rate of 0.1 mV s^{-1}. (e) Rate performance and (f) cycling stability of Bi_2S_3 HS and Bi_2S_3-PPy HS.

surface of Bi_2S_3 HS becomes rough and its inner is hollow (Fig. 3c,d and S3c,d). While for Bi_2S_3-PPy HS, hollow Bi_2S_3 is coated with a thin layer of PPy with a thickness of 10 nm (Fig. 3e,f and S3e,f). Selected-area electron diffraction (SAED) in inset of Fig. 3e also proves the amorphous characterization of Bi_2S_3-PPy HS. Furthermore, the elemental mappings reveal the PPy coating and hollow structure in Bi_2S_3-PPy HS (Fig. 3g-l). The above analyses and results verify the successful fabrication of amorphous Bi_2S_3-polypyrrole hollow sphere. The electrochemical tests in SIB are performed in a 2032-type coin cell using sodium foil as counter and reference electrode. Fig. 4a displays Nyquist plots of Bi_2S_3 HS and Bi_2S_3-PPy HS (fresh cell) and an equivalent electrical circuit is showed in Fig. S4. The charge transfer resistance (R_{ct}) calculated from semi-circle in high-frequency region of Bi_2S_3-PPy HS (5 Ω) is obviously smaller than that of Bi_2S_3 HS (12 Ω) due to the good conductivity of PPy. The Warburg impedance in low-frequency region reflects the sodium ion transfer rate from the electrolyte to the electrode surface.[45, 46] The large slope of Bi_2S_3 HS indicates the fast sodium ion transfer, resulting from the hollow structure with large specific surface area. The close slopes between Bi_2S_3 HS (67˚) and Bi_2S_3-PPy HS (71˚) indicate that the PPy coating does not weaken the sodium ion transfer. The 1st and 2nd charging-discharging curves of Bi_2S_3 HS and Bi_2S_3-PPy HS are exhibited in Fig. 4b. The same discharging plateaus demonstrate their same sodiation/desodiation mechanism. While the discharging capacities of Bi_2S_3-PPy HS are larger than those of Bi_2S_3 HS. The 1st and 2nd discharging capacities of Bi_2S_3-PPy HS (Bi_2S_3 HS) are 549.7 (500.2) and 409.1 (348.2) mAh g^{-1} respectively. The cyclic voltammetry (CV) tests of Bi_2S_3 HS and Bi_2S_3-PPy HS are conducted to further reveal charging-discharging mechanism (Fig. 4c,d and S5). They also exhibit same redox peaks. For the first cycle, the reduction peaks at 1.35 and 1.06 V are due to the generation of solid electrolyte interface (SEI) film and the conversion reaction of amorphous Bi_2S_3 into metallic Bi and Na_2S (Fig. 4c).[47] The characteristic peaks at 0.62 and 0.40 V are ascribed to the sodiation reaction of Bi, i. e., $Bi + Na^+ + e^- \rightarrow NaBi$ and $NaBi + 2Na^+ + 2e^- \rightarrow Na_3Bi$.[36, 37, 48, 49] The cathodic peak at 0.27 V originates from the sodiation of PVP. Only two oxidation peaks at 0.62 and 0.75 V, corresponding to the sodium deintercalation reaction of Na_3Bi, can be seen, which suggests that Bi cannot convert into amorphous Bi_2S_3 during electrooxidation process.[36, 37, 48, 49] During the following cycles, the peak at 0.27 V decays gradually and disappears finally (Fig. 4d). The redox couples of 0.38/0.61 and 0.57/0.75 V are attributed to the sodiation/desodiation of Bi.[36, 37, 48, 49] The conclusion is that the main active material is Bi in SIB. The XRD patterns of Bi_2S_3-PPy HS after 1 and 5000 cycles are collected, as shown in Fig. S6. The strong characteristic peaks of metallic Bi (PDF#44-1246) can be observed, further proving the above conclusion. Noted that the intensity of 0.38/0.61 redox couples increases with the increasing scan rates while there is a small potential variation, demonstrating the weak polarization of Bi_2S_3-PPy HS during charging/discharging process.[50] Moreover, the discharging curves at different current densities of Bi_2S_3-PPy HS show a stable plateau at about 0.43 V (Fig. S7).

Fig. 4e,f show the rate performance and cyclic stability. The discharging capacities of Bi_2S_3-PPy HS are 365, 350, 329, 301 and 278 mAh g^{-1} at the current densities of 100, 500, 1000, 2000, and 3000 mA g^{-1}, which obviously outperforms those of Bi_2S_3 HS (308, 270, 237, 161 and 104 mAh g^{-1}) as exhibited in Fig. 4e. Compared to Bi_2S_3 HS (34%), a higher capacity retention of Bi_2S_3-PPy HS (76%) is obtained as the current density increases from 100 to 3000 mA g^{-1}, reflecting its outstanding rate performance. This is due to the hollow structure and the PPy coating with good conductivity, resulting in the accelerated charge transfer.[28] Meanwhile, Bi_2S_3-PPy HS shows a better cyclic stability with 90% capacity retention of second cycle after 5000 cycles at 1000 mA g^{-1} (Fig. 4f). By contrast, only 40% capacity retention can be obtained for Bi_2S_3 HS. The long-term durability of Bi_2S_3-PPy HS is ascribed to the inactive PPy coating effectively preventing the electrode pulverization and the hollow structure providing the enough space for volume change during sodium intercalation and deintercalation process.[28] Meanwhile, we compare the cycling performances of Bi_2S_3-PPy HS and the previously reported Bi-based electrodes, as seen in Table S1. The long cyclic life and high capacity retention of Bi_2S_3-PPy HS exceed those of most electrodes. The initial low coulombic efficiency (70%) results from the irreversible conversion reaction of amorphous Bi_2S_3 and the formation of SEI. While the high coulombic efficiency can be obtained during the following cyclic tests. After cyclic test, Bi_2S_3-PPy HS still has a smaller R_{ct} compared to Bi_2S_3 HS (Fig. S8). Meanwhile, the Warburg resistance of Bi_2S_3-PPy HS after cycling is far below that of Bi_2S_3 HS after cycling. This is because the PPy coating prevents the collapse of hollow structure. The electrochemical kinetics can be analyzed by the following equation:[36]

$$i=av^b \quad (1)$$

where i is peak current, v is scan rate. a and b can be obtained from the intercept and slope of log(i)-log(v) plots. If b=0.5, a diffusion-controlled faradaic intercalation process is reflected, while a b value of 1 reveals a surface-controlled capacitive process.[36] The CV curves at different scan rates of Bi_2S_3 HS and Bi_2S_3-PPy HS are exhibited in Fig. S9a,b. The slope of peak 1 is ca. 0.5, indicating a typical faradaic intercalation process of Bi_2S_3 HS (Fig. S9c). For the peak 2 of Bi_2S_3-PPy HS, the b value of ca. 0.7 reveals a portion of pseudocapacitive process, resulting in a faster charge storage than that of Bi_2S_3 HS.

Another application of Bi_2S_3-PPy HS in Li-S battery is performed using Li as counter and reference electrode. The XRD patterns of sulfur, Bi_2S_3 HS/S and Bi_2S_3-PPy HS/S are showed in Fig. 5a. The successful sulfur infiltration is demonstrated by the distinct characteristic peaks of S_8 (PDF#08-0247) in Bi_2S_3 HS/S and Bi_2S_3-PPy HS/S. TEM images of Bi_2S_3 HS/S and Bi_2S_3-PPy HS/S suggest that the inner space of both is filled with sulfur (Fig. 5b,c). SAED proves the existence of sulfur with single-crystalline property (inset of Fig. 5c). The elemental mappings of Bi_2S_3-PPy HS/S composite show the even distribution of C, N, Bi and S. Compared with Bi_2S_3-PPy HS (Fig. 3g-l), the hollow structure of Bi_2S_3-PPy HS/S cannot be identified, indicating the sulfur occupancy in the hollow space (Fig. S10). The N_2 adsorption-desorption isotherms, pore size distribution and cumulative pore volume plots of Bi_2S_3-PPy HS and Bi_2S_3-PPy HS/S are

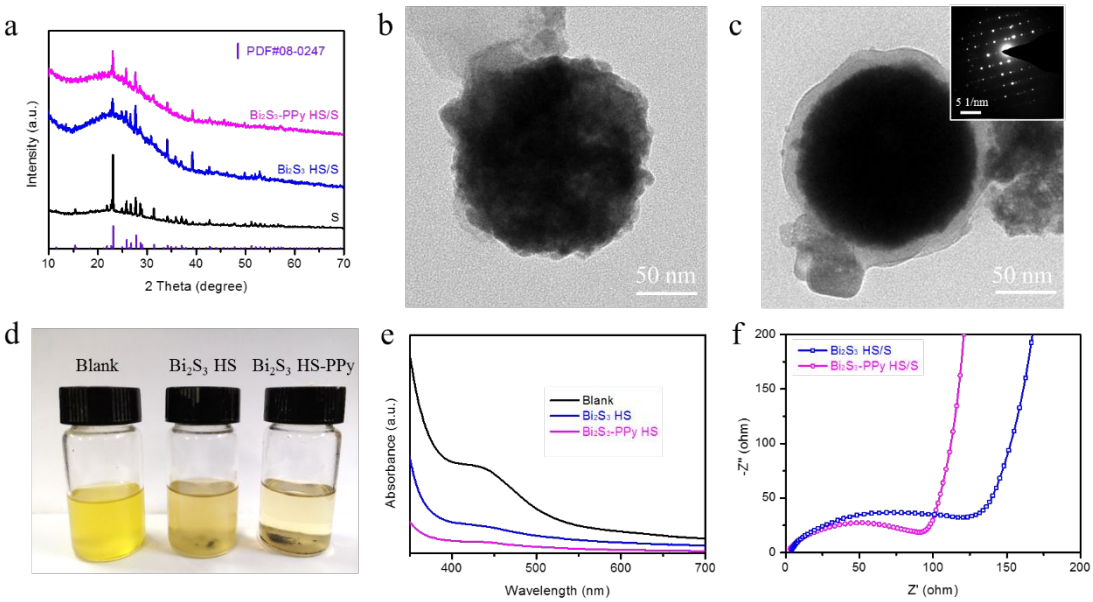

Fig. 5 (a) XRD patterns of S, Bi_2S_3 HS/S and Bi_2S_3-PPy HS/S. TEM images of (b) Bi_2S_3 HS/S and (c) Bi_2S_3-PPy HS/S and inset of (c) is SAED image. (d) Digital photographs and (e) UV-vis spectra of Li_2S_6, Li_2S_6 with Bi_2S_3 HS and Li_2S_6 with Bi_2S_3-PPy HS solutions after adsorption for 2 h. (f) EIS spectra of Bi_2S_3 HS/S and Bi_2S_3-PPy HS/S.

showed in Fig. S11. The specific surface areas of Bi_2S_3-PPy HS and Bi_2S_3-PPy HS/S are 0.6864 and 0.0638 m^2 g^{-1}. Meanwhile, the number of hole and the cumulative pore volume of Bi_2S_3-PPy HS are much bigger than those of Bi_2S_3-PPy HS/S. These reveal that the most pores have been occupied by sulfur after the sulfur infiltration. The thermogravimetric analysis (TGA) curves of Bi_2S_3-PPy HS and Bi_2S_3-PPy HS/S are collected to present the fractions of Bi_2S_3, PPy and S in the Bi_2S_3-PPy HS/S, as displayed in Fig. S12. The detailed analysis can be seen in Supporting Information. The fractions of H_2O, Bi_2S_3, PPy and S in the Bi_2S_3-PPy HS/S composite are about 1.4%, 29.4%, 5.2% and 64.0%. To obtain an excellent cathode with long cyclic life, the suppression of the dissolution and the "shuttle effect" of LiPSs in electrolyte is extremely important. Apart from the physical adsorption of outer double layer structure, Bi_2S_3 and PPy with the polar bonds (such as Bi-S and C-N) also can dramatically adsorb LiPSs by chemical binding with LiPSs.[51, 52] A comparison of adsorption capability for Li_2S_6 is displayed in Fig. 5d. 20 mg Bi_2S_3 HS and Bi_2S_3-PPy HS are added into the 10 mL yellow Li_2S_6 solution (3 mmol L^{-1}) respectively. After 2 h, the color of Li_2S_6 solution with Bi_2S_3 HS turns faint yellow. By comparison, the solution with Bi_2S_3-PPy HS is almost colorless. To further estimate the adsorption ability of samples for Li_2S_6, the UV-vis spectroscopy of above solutions is collected (Fig. 5e). The blank Li_2S_6 solution has a strong absorbance in the range from 400 to 500 nm, which is stronger than the solution with Bi_2S_3 HS. While the light absorbance of solution with Bi_2S_3-PPy HS is ignorable, indicating that Bi_2S_3-PPy HS has a stronger affinity for LiPSs than Bi_2S_3 HS. Furthermore, owing to the excellent conductivity of PPy, the R_{ct} of Bi_2S_3-PPy HS/S is much less than that of Bi_2S_3 HS/S (Fig. 5f). These advantages of Bi_2S_3-PPy HS/S suggest that it should have the better electrochemical properties than Bi_2S_3 HS/S in Li-S battery.

As seen in Fig. 6a,b, the 1st discharging capacity of Bi_2S_3 HS/S is up to 2095 mAh g^{-1}, higher than that of Bi_2S_3-PPy HS/S (1772 mAh g^{-1}). While the 2nd and 3rd discharging capacities of Bi_2S_3 HS/S are lower than those of Bi_2S_3-PPy HS/S (Fig. 6a,b). The slower capacity fading of Bi_2S_3-PPy HS/S proves the function of PPy coating for preventing the loss of LiPSs. The discharging plateaus at about 2.30 and 2.12 V are ascribed to the formation of long-chain polysulfides (Li_2S_x, $4 \le x \le 8$) and short-chain polysulfides (Li_2S_x, $1 \le x \le 4$), respectively.[29, 32] Compared to Bi_2S_3 HS/S (0.20 V), the narrower potential gap of Bi_2S_3-PPy HS/S (0.11 V) between charging and discharging plateaus demonstrates its decreased polarization and elevated electrochemical reaction kinetics.[12, 53] Noted that the 1st discharging capacities of both Bi_2S_3 HS/S and Bi_2S_3-PPy HS/S surpass the theoretical capacity of pure S (1675 mAh g^{-1}) and an extra discharging plateau at about 1.73 V can be seen. Similar results also can be seen in CV curves (Fig. 6c). A pair of unreported redox peak at 1.62/2.61 V occurs, which is not found in previous sulfur-based cathode such as S, Li_2S and S-rich copolymer.[50, 54-56] This indicates that more Li^+ intercalation to S is achieved and brings an additional discharging capacity. Meanwhile, it is found that the discharging capacity of Bi_2S_3 HS without sulfur as cathode of Li-S battery is ignorable and there is not visible plateau at about 1.73 V, revealing that Bi_2S_3 does not take part in energy storage process in Li-S battery test (Fig. S13). Therefore, this plateau can be attributed to the residual PVP in preparation process of Bi_2S_3 HS. The XRD patterns and XPS spectra reflect the chemical combination of PVP and S after the heating treatment (the preparation method of PVP/S can be seen in experimental section). As exhibited in Fig. 6d, there is not distinct characteristic peak for PVP and PVP after heat treatment (PVP-ht), while PVP/S displays several characteristic peaks at 28.5°, 29.2°, 30.7° 39.7°, 41.0° and 50.9°, which are different from S_8 (PDF#08-0247) or other allotropes. The S 2p XPS spectra prove

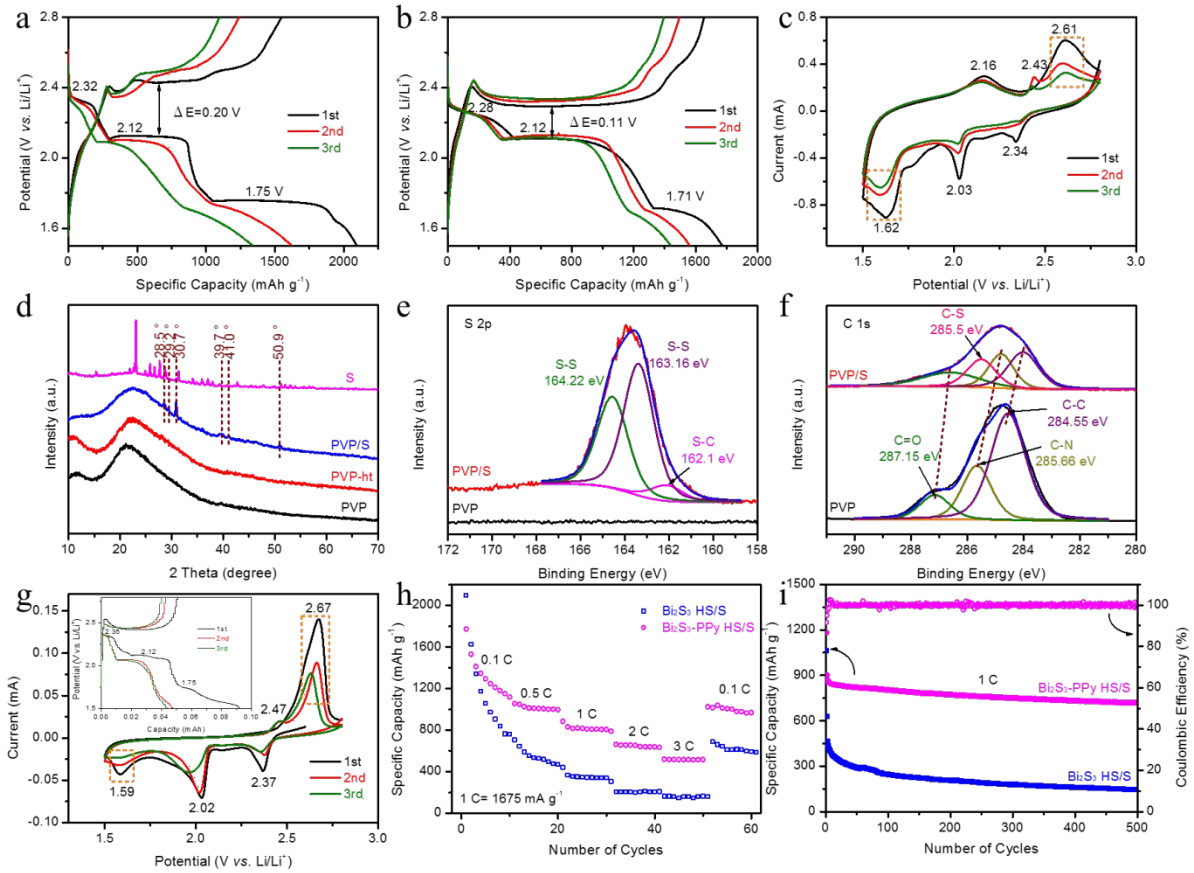

Fig. 6 The 1st-3rd charging-discharging curves of (a) Bi_2S_3 HS/S and (b) Bi_2S_3-PPy HS/S. (c) CV curves of Bi_2S_3 HS/S at 0.1 mV s^{-1}. (d) XRD patterns of PVP, PVP-ht, PVP/S and S. (e) S 2p and (f) C 1s spectra of PVP and PVP/S. (g) CV and charging-discharging (inset) curves of PVP/S at 0.1 mV s^{-1}. (h) Rate capability and (i) cyclic life of Bi_2S_3 HS/S and Bi_2S_3-PPy HS/S.

the existence of elemental sulfur and S-C bond (162.1 eV) in PVP/S (Fig. 6e).[55] Moreover, an additional C-S bond (285.5 eV) can be seen and the distinct peaks shift of C-C, C-N and C=O can be seen in comparison with C 1s spectrum of PVP (Fig. 6f).[56] Furthermore, the charging-discharging and CV curves of PVP/S display the same discharging plateaus (1.75 V) and redox peaks (1.59/2.67 V) as those of Bi_2S_3 HS/S (Fig. 6g). All of these suggest that PVP is combined with S by chemical bond. This finding provides a reference for fabricating S-rich copolymer cathode of Li-S battery.

The rate performance is tested at different current densities (Fig. 6h). Bi_2S_3-PPy HS/S shows a high rate performance with the discharging capacities of 1293, 1005, 809, 648 and 515 mAh g^{-1} at current densities of 0.1, 0.5, 1, 2 and 3 C, markedly higher than those of Bi_2S_3 HS/S (1051, 538, 348, 212 and 158 mAh g^{-1}). When the current density is set back to 0.1 C, compared to Bi_2S_3 HS/S (624 mAh g^{-1}), a high reversible capacity of 1008 mAh g^{-1} for Bi_2S_3-PPy HS/S can be obtained. The excellent rate capability of Bi_2S_3-PPy HS/S is due to the rapid charge transfer resulting from the hollow structure of Bi_2S_3 and the good conductivity of PPy. Further cycling stability is studied, as seen in Fig. 6i. Bi_2S_3-PPy HS/S delivers an initial capacity of 1180 mAh g^{-1} and a reversible capacity of 729 mAh g^{-1} after 500 cycles at 1 C. By comparison, Bi_2S_3 HS/S offers an initial capacity of 1060 mAh g^{-1} and a low capacity of 146 mAh g^{-1} after 500 cycles. The poor cycling life of Bi_2S_3 HS/S is due to the expansion of inner S bursting Bi_2S_3 HS and the dissolution of LiPSs. The long-term durability of Bi_2S_3-PPy HS/S is attributed to the double-layer protection of Bi_2S_3-PPy HS which confines the "shuttle effect" and the dissolution of LiPSs as well as the volume variation of inner sulfur during charging and discharging process. There is rarely report using Bi_2S_3-PPy composite as S host for a long life lithium-sulfur battery. Moreover, the cyclic test of Bi_2S_3-PPy HS/S with a high sulfur loading (5.2 mg cm^{-2}) is conducted. As depicted in Fig. S14, a high reversible capacity of 643 mAh g^{-1} after 200 cycles is obtained, demonstrating the potential of Bi_2S_3-PPy HS/S in the practical application of Li-S battery.

Conclusions

In summary, a PPy coated amorphous Bi_2S_3 hollow sphere is fabricated by sulfurating BiG sphere with PPy coating and applied in both SIB and Li-S battery. The conductive PPy layer and hollow structure resulting from Kirkendall Effect accelerate the charge transfer, tolerate the electrode pulverization and dramatically adsorb the LiPSs. Thus, Bi_2S_3-PPy HS exhibits excellent rate performance with a reversible capacity of 278 mAh g^{-1} at 3000 mA g^{-1} and long cycling life with 90% capacity retention of second cycle after 5000 cycles at 1000 mA g^{-1} in SIB. For Li-S battery, this multifunctional electrode also shows an

outstanding electrochemical properties with a high initial capacity (1772 mAh g^{-1}) exceeding theoretical capacity, a discharging capacity of 729 mAh g^{-1} after 500 cycles at 1 C. This work supplies reference for the design of excellent multifunctional electrode material in energy storage systems.

Materials and methods

Preparation of BiG sphere

First, 1.5 mmol $Bi(NO_3)_3 \cdot 5H_2O$ was dissolved into 20 mL 1 mol L^{-1} HNO_3, then 0.12 mmol PVP and 100 mL glycol were added into the above solution and stirred for 1 h. The resultant transparent solution was transferred into a Teflon-lined stainless steel autoclave and heated in an oven at 150 °C for 12 h. To obtain Bi-glycol (BiG) sphere, the products were centrifuged, washed and dried.

Preparation of Bi_2S_3-PPy HS

To grow an even layer of PPy onto the surface of BiG sphere, 0.24 g BiG sphere and 20 mg sodium dodecyl benzene sulfate were added into 240 mL H_2O and dispersed by an ultrasonic instrument. The solution was further stirred for 10 h. 0.07 mL pyrrole, 2 mL 1 mol L^{-1} HCl and 20 mL 0.01 mol L^{-1} ammonium persulphate aqueous solution were successively added into the above solution and stirred for 3 h in an ice-water bath. The products (BiG sphere-PPy) were centrifuged, washed and dried. During sulfuration process, the dried products (0.1 g) were dispersed in a 20 mL 0.5 mol L^{-1} Na_2S aqueous solution and stirred for 1 h. The final product is labeled as Bi_2S_3-PPy HS. For comparison, Bi_2S_3 HS was prepared by the sulfuration of BiG sphere.

Preparation of Bi_2S_3 HS/S, Bi_2S_3-PPy HS/S and PVP/S

The as-synthesized Bi_2S_3-PPy HS (Bi_2S_3 HS) and sulfur (Aldrich, 99.995%) were thoroughly mixed with a mass ratio of 3:7. The mixture was first heated to 155 °C for 10 h in a sealed vessel filled with argon gas to ensure a complete infiltration of sulfur into hollow sphere and then heated to 300 °C for 30 min to sublimate superfluous sulfur. After cooling down, the Bi_2S_3-PPy HS/S (Bi_2S_3 HS/S) composite was obtained. The mass fraction of sulfur in Bi_2S_3-PPy HS (Bi_2S_3 HS) is about 62% (64%).

The mixture of PVP and sulfur (1:1, m/m) was processed in the same heating condition. The product is labled as PVP/S as a control sample.

Preparation of Li_2S_6

Li_2S and S with a mole ratio of 1:5 were added into a mixed solution (1:1, v/v) containing 1,3-dioxolane (DOL) and 1,2-dimethoxyethane (DME). This solution was stirred at 70 °C for 12 h to prepare a 0.25 mol L^{-1} yellow Li_2S_6 solution. Before the adsorption experiment, this solution was diluted to 3 mmol L^{-1}.

Characterization

The crystal structure, molecular structure and elemental composition were analyzed by X-ray diffraction (XRD, D-MAX 2200 VPC, Rigaku) with Cu Kα radiation (λ = 1.5418 A), Raman spectra (inVia, Renishaw) with a laser length of 514 nm and X-ray photoelectron spectroscopy (XPS, ESCALab250, Thermo VG) corrected by C 1s line at 284.6 eV. Scanning electron microscope (SEM, Gemini500, Zeiss) and transmission electron microscope (TEM, Tecnai G2 F30, FEI) were utilized to obverse the morphology of samples. The thermogravimetric analysis (TGA, TG-209, Netzsch) was performed to determine the fractions of each constituent. N_2 adsorption-desorption isotherms (ASAP2460, Micromeritics) were measured to obtain the specific surface area, the pore size distribution and the pore volume of samples.

Electrochemical measurements

The half-cell tests were performed in a 2032-type coin cell. Na and Li foil were used as counter electrode of SIB and Li-S battery. The separator was microporous polypropylene film. For SIB, the electrolyte was DME solution with 1 mol L^{-1} $NaPF_6$. For Li-S battery, the electrolyte was a mixed solvent of DOL and DME (1:1 v/v) with 1 mol L^{-1} lithium bis(trifluoromethane sulfonyl)imide (LiTFSI) and 2% $LiNO_3$. The electrolyte/sulfur ratio in Li-S cells is 15 μL mg^{-1}. The working electrodes were prepared by casting the slurry containing 80% active material, 10% acetylene black, and 10% poly(vinylidene fluoride) onto a Cu/Al foil current collector. The mass loadings of Bi_2S_3-PPy HS for SIB and S for Li-S battery were 1.5 and 1.2 mg cm^{-2}, respectively. The cell tests were carried out in the voltage window of 0.01-2.0 V (SIB) and 1.5-2.8 V (Li-S battery) by a LANHE battery testing system (Wuhan, China). CHI1040c and CHI760e electrochemical workstation were used to obtain cyclic voltammetry (CV) curves and electrochemical impedance spectra (EIS, Frequency: 0.1-100000 Hz).

Conflicts of interest

There are no conflicts to declare.

Acknowledgements

This work was supported by the National Key Research and Development Program of China (2016YFA0202604), the Natural Science Foundation of China (21773315 and 21576056), the Science and Technology Plan Project of Guangdong Province (2015B010118002), the Fundamental Research Funds for the Central Universities (17lgjc36), the Science and Technology Plan Project of Guangzhou, China (201604010124 and 201804020025), Guangdong Natural Science Foundation (2017A030311016), Guangdong Provincial Key Platform and Major Scientific Research Projects for Colleges and Universities (2015KCXTD029), the Tip-top Scientific and Technical Innovative Youth Talents of Guangdong special support program (2016TQ03N322), China plans to introduce Foreign Talents to Major National Science and Technology Projects (ZD20180029).and Local Innovative and Research Teams Project of Guangdong Pearl River Talents Program.

References

1. D. Chao, C. Zhu, P. Yang, X. Xia, J. Liu, J. Wang, X. Fan, S. V. Savilov, J. Lin, H. J. Fan and Z. X. Shen, *Nat. Commun.*, 2016, **7**, 12122.
2. S. Song, V. Maragou, P. Tsiakaras, *J. Fuel Cell Sci. Technol.*, 2007, **4**, 203.
3. Q. Zhou, L. Liu, Z. Huang, L. Yi, X. Wang and G. Cao, *J. Mater. Chem. A*, 2016, **4**, 5505.
4. B. Long, M. S. Balogun, L. Luo, W. Qiu, Y. Luo, S. Song and Y. Tong, *Adv. Energy Mater.*, 2018, **8**, 1701681.
5. S. Song, J. Liu, J. Shi, H. Liu, V. Maragou, Y. Wang, P. Tsiakaras, *Appl. Cata. B: Environ.*, 2011, **103**, 287.
6. M.-S. Balogun, Y. Huang, W. Qiu, H. Yang, H. Ji and Y. Tong, *Mater. Today*, 2017, **20**, 425.
7. B. Long, M. S. Balogun, L. Luo, Y. Luo, W. Qiu, S. Song, L. Zhang and Y. Tong, *Small*, 2017, **13**, 1702081.
8. H. Li, Y. Ding, H. Ha, Y. Shi, L. Peng, X. Zhang, C. J. Ellison and G. Yu, *Adv. Mater.*, 2017, **29**, 1804271.
9. M.-S. Balogun, H. Yang, Y. Luo, W. Qiu, Y. Huang, Z.-Q. Liu and Y. Tong, *Energy Environ. Sci.*, 2018, **11**, 1859.
10. C. Wu, P. Kopold, P. A. Van Aken, J. Maier and Y. Yu, *Adv. Mater.*, 2017, **29**, 1604015.
11. P. F. Wang, Y. J. Guo, H. Duan, T. T. Zuo, E. Hu, K. Attenkofer, H. Li, X. S. Zhao, Y. X. Yin and X. Yu, *ACS Energy Lett.*, 2017, **2**, 2715.
12. J. Zhang, Y. Shi, Y. Ding, L. Peng, W. Zhang and G. Yu, *Adv. Energy Mater.*, 2017, **7**, 1602876.
13. X. Wang, G. Li, J. Li, Y. Zhang, A. Wook, A. Yu and Z. Chen, *Energy Environ. Sci.*, 2016, **9**, 2533.
14. P. Xiao, F. Bu, G. Yang, Y. Zhang and Y. Xu, *Adv. Mater.*, 2017, **29**, 1703324.
15. W. Zhou, L. Xue, X. Lu, H. Gao, Y. Li, S. Xin, G. Fu, Z. Cui, Y. Zhu and J. B. Goodenough, *Nano Lett.*, 2016, **16**, 7836.
16. Y. Zhao, L. V. Goncharova, Q. Zhang, P. Kaghazchi, Q. Sun, A. Lushington, B. Wang, R. Li and X. Sun, *Nano Lett.*, 2017, **17**, 5653.
17. J. Xia, L. Liu, S. Jamil, J. Xie, H. Yan, Y. Yuan, Y. Zhang, S. Nie, J. Pan, X. Wang and G. Cao, *Energy Stor. Mater.*, 2018, DOI: 10.1016/j.ensm.2018.08.005.
18. W. Li, M. Li, K. R. Adair, X. Sun and Y. Yu, *J. Mater. Chem. A*, 2017, **5**, 13882.
19. Y. Wang, D. Adekoya, J. Sun, T. Tang, H. Qiu, L. Xu, S. Zhang and Y. Hou, *Adv. Funct. Mater.*, 2018, DOI: 10.1002/adfm.201807485.
20. G. Li, Q. Huang, X. He, Y. Gao, D. Wang, S. H. Kim and D. Wang, *ACS Nano*, 2018, **12**, 1500.
21. D.-R. Deng, J. Lei, F. Xue, C.-D. Bai, X.-D. Lin, J.-C. Ye, M.-S. Zheng and Q.-F. Dong, *J. Mater. Chem. A*, 2017, **5**, 23497.
22. L. Shen, H. Lv, S. Chen, P. Kopold, P. A. V. Aken, X. Wu, J. Maier and Y. Yu, *Adv. Mater.*, 2017, **29**, 1700142.
23. B. Zhang, C. M. Ghimbeu, C. Laberty, C. Vix‐Guterl and J. M. Tarascon, *Adv. Energy Mater.*, 2016, **6**, 1501588.
24. J. Mao, T. Zhou, Y. Zheng, H. Gao, H. K. Liu and Z. Guo, *J. Mater. Chem. A*, 2018, **6**, 3284.
25. H. Tian, T. Wang, F. Zhang, S. Zhao, S. Wan, F. He and G. Wang, *J. Mater. Chem. A*, 2018, **6**, 12816.
26. Q. Zhu, Q. Zhao, Y. An, B. Anasori, H. Wang and B. Xu, *Nano Energy*, 2017, **33**, 402.
27. Q. Zhu, X. Chang, N. Sun, R. Chen, Y. Zhao, B. Xu and F. Wu, *ACS Appl. Mater. Interfaces*, 2019, **11**, 3107.
28. H. Park, J. Kwon, H. Choi, D. Shin, T. Song and X. W. D. Lou, *ACS Nano*, 2018, **12**, 2827.
29. Y. Zhong, X. Xia, S. Deng, J. Zhan, R. Fang, Y. Xia, X. Wang, Q. Zhang and J. Tu, *Adv. Energy Mater.*, 2018, **8**, 1701110.
30. Z. Liu, T. Lu, T. Song, X.-Y. Yu, X. W. Lou and U. Paik, *Energy Environ. Sci.*, 2017, **10**, 1576.
31. J. Chen, S. Li, V. Kumar and P. S. Lee, *Adv. Energy Mater.*, 2017, **7**, 1700180.
32. S. Mei, C. J. Jafta, I. Lauermann, Q. Ran, M. Kärgell, M. Ballauff and Y. Lu, *Adv Funct. Mater.*, 2017, **27**, 1701176.
33. Y. Liu, N. Zhang, L. Jiao, Z. Tao and J. Chen, *Adv. Funct. Mater.*, 2015, **25**, 214.
34. J.-Y. Hwang, S.-T. Myung and Y.-K. Sun, *Chem. Soc. Rev.*, 2017, **46**, 3529.
35. H. Gao, J. Niu, C. Zhang, Z. Peng and Z. Zhang, *ACS Nano*, 2018, **12**, 3568.
36. J. Chen, X. Fan, X. Ji, T. Gao, S. Hou, X. Zhou, L. Wang, F. Wang, C. Yang, L. Chen and C. Wang, *Energy Environ. Sci.*, 2018, **11**, 1218.
37. C. Wang, L. Wang, F. Li, F. Cheng and J. Chen, *Adv. Mater.*, 2017, **29**, 1702212.
38. T. Lei, W. Chen, J. Huang, C. Yan, H. Sun, C. Wang, W. Zhang, Y. Li and J. Xiong, *Adv. Energy Mater.*, 2017, **7**, 1601843.
39. J. He, Y. Chen and A. Manthiram, *Energy Environ. Sci.*, 2018, **11**, 2560.
40. S. Biswas, A. Mondal, D. Mukherjee and P. Pramanik, *J. Electrochem. Soc.*, 1986, **17**, 48.
41. S. H. Yu, J. Yang, Y. S. Wu, Z. H. Han, Y. Xie and Y. T. Qian, *Mater. Res. Bull.*, 1998, **33**, 1661.
42. Y. Wang, J. Chen, L. Jiang, K. Sun, F. Liu and Y. Lai, *J. Alloy Compd.*, 2016, **686**, 684.
43. A. Jana, C. Bhattacharya and J. Datta, *Electrochim. Acta*, 2010, **55**, 6553.
44. J. X. Feng, H. Xu, S. H. Ye, G. Ouyang, Y. X. Tong and G. R. Li, *Angew. Chem. Int. Ed.*, 2017, **56**, 8120.
45. B. Long, H. Yang, F. Wang, Y. Mao, M.-S. Balogun, S. Song and Y. Tong, *Electrochim. Acta*, 2018, **284**, 271.
46. B. Long, L. Luo, J. Zhang, M.-S. Balogun, S. Song and Y. Tong, *Mater. Today Energy*, 2018, **9**, 311.
47. W. Sun, X. Rui, D. Zhang, Y. Jiang, Z. Sun, H. Liu and S. Dou, *J. Power Sources*, 2016, **309**, 135.
48. D. Su, S. Dou and G. Wang, *Nano Energy*, 2015, **12**, 88.
49. H. Gao, W. Ma, W. Yang, J. Wang, J. Niu, F. Luo, Z. Peng and Z. Zhang, *J. Power Sources*, 2018, **379**, 1.
50. J. Zhang, Y. Shi, Y. Ding, W. Zhang and G. Yu, *Nano Lett.*, 2016, **16**, 7276.
51. X. Liang, M. Zhang, M. R. Kaiser, X. Gao, K. Konstantinov, R. Tandiono, Z. Wang, H.-K. Liu, S.-X. Dou and J. Wang, *Nano Energy*, 2015, **11**, 587.
52. Y. Liu, W. Yan, X. An, X. Du, Z. Wang, H. Fan, S. Liu, X. Hao and G. Guan, *Electrochim. Acta*, 2018, **271**, 67.
53. F. Wu, T. P. Pollard, E. Zhao, Y. Xiao, M. Olguin, O. A. Borodin and G. Yushin, *Energy Environ. Sci.*, 2018, **11**, 807.
54. L. Qie and A. Manthiram, *ACS Energy Lett.*, 2016, **1**, 46.
55. G. Hu, Z. Sun, C. Shi, R. Fang, J. Chen, P. Hou, C. Liu, H. M. Cheng and F. Li, *Adv. Mater.*, 2017, **29**, 1603835.
56. A. Ghosh, S. Shukla, M. Monisha, A. Kumar, B. Lochab and S. Mitra, *ACS Energy Lett.*, 2017, **2**, 2478.

TOC

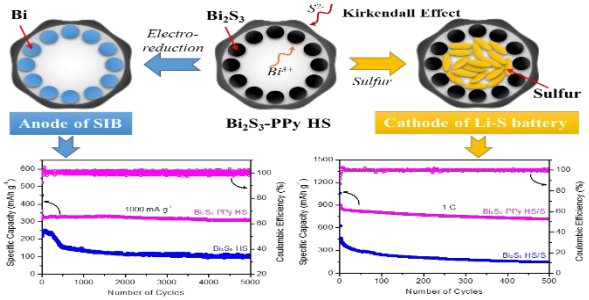

The well-designed amorphous Bi_2S_3-polypyrrole core-shell hollow sphere shows excellent electrochemical properties in both SIB and Li-S battery.